

Quantum control of a single H_2^+ molecular ion

D. Holzapfel,^{1,2,*} F. Schmid,^{1,2} N. Schwegler,^{1,2} O. Stadler,¹
M. Stadler,^{1,2} A. Ferk,^{1,2} J. P. Home,^{1,2} and D. Kienzler^{1,2,†}

¹Department of Physics, ETH Zürich, Zurich, Switzerland

²Quantum Center, ETH Zürich, Zurich, Switzerland

Science is founded on the benchmarking of theoretical models against experimental measurements, with the challenge that for all but the simplest systems, the calculations required for high precision become extremely challenging. H_2^+ is the simplest stable molecule, and its internal structure is calculable to high precision from first principles [1]. This allows tests of theoretical models and the determination of fundamental constants [2]. However, studying H_2^+ experimentally presents significant challenges. Standard control methods such as laser cooling, fluorescence detection and optical pumping are not applicable to H_2^+ due to the very long lifetimes of its excited rotational and vibrational states. Here we solve this issue by using Quantum Logic Spectroscopy techniques to demonstrate full quantum control of a single H_2^+ molecule by co-trapping it with an atomic ‘helper’ ion and performing quantum operations between the two ions [3]. This enables us to perform pure quantum state preparation, coherent control and non-destructive readout, which we use to perform high-resolution microwave spectroscopy of H_2^+ . Our results pave the way for high precision spectroscopy of H_2^+ in both the microwave and optical domains, while offering techniques which are transferable to other molecular ions.

The H_2^+ ion is the simplest molecule and therefore an important system to test current theory, determine fundamental constants, and to search for new physics [2, 4, 5]. However, it is very difficult to study experimentally, and as a result only little high-precision data exists so far. Recently two experiments have demonstrated high-precision rotational and vibrational spectroscopy of H_2^+ for the first time, using molecular ensembles [6, 7]. Eventually, ensemble experiments will likely be limited by systematic uncertainties. In contrast, spectroscopy of single trapped ions, one of the most precise measurement tools in physics, can achieve much lower uncertainties, exemplified by atomic-ion-based optical clocks [8, 9]. Spectroscopy of a single trapped H_2^+ ion is expected to allow for the most precise measurements of its internal structure [10–12]. Experiments with single ions are enabled by quantum control techniques such as laser cooling, pure quantum state preparation, coherent control,

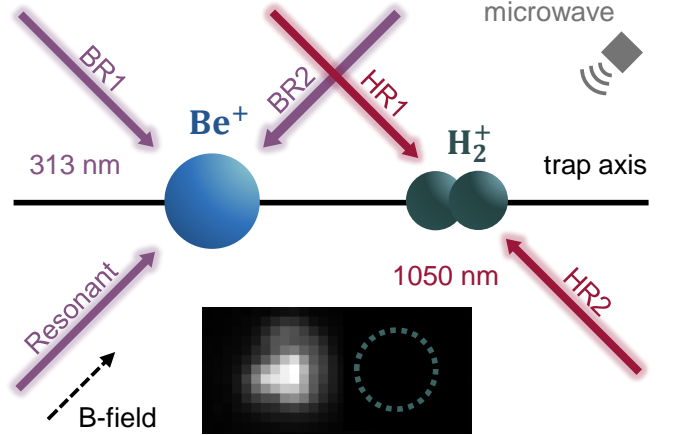


Figure 1. **Sketch of H_2^+ – ${}^9\text{Be}^+$ ion pair and beam geometry.** A single ${}^9\text{Be}^+$ and a single H_2^+ ion are simultaneously confined in a linear Paul trap and align along the trap axis. A magnetic field (\mathbf{B}) with strength $450\ \mu\text{T}$ defines the quantization axis with an angle of 45° with regard to the trap axis. The laser beams addressing ${}^9\text{Be}^+$ at $313\ \text{nm}$ are shown in purple. The ‘Resonant’ beam is propagating in parallel to the direction of the magnetic field and is used for laser cooling, state preparation and fluorescence detection of ${}^9\text{Be}^+$. The ${}^9\text{Be}^+$ Raman beam pair consists of the ‘BR1’ and ‘BR2’ beams. The H_2^+ Raman beam pair at $1050\ \text{nm}$ (‘HR1’, ‘HR2’) is shown in red. A microwave drives magnetic dipole transitions in the hyperfine structure of both ions. The inset shows a picture capturing the fluorescence of the ${}^9\text{Be}^+$ ion (left), while the H_2^+ ion (right) at a distance of $8.6\ \mu\text{m}$ remains invisible. The estimated position of the H_2^+ ion is indicated by a dotted circle.

and non-destructive readout. A direct implementation requires a suitable electronic structure, which H_2^+ lacks. Quantum Logic Spectroscopy (QLS) has been developed to implement quantum control for atomic or molecular ion species without such structure [3, 13]. In QLS, a well controlled atomic ion is co-trapped with the ion of interest, and quantum logic operations that utilize their mutual Coulomb interaction enable full control over the ion of interest. QLS has recently been implemented for the molecular ions MgH^+ , CaH^+ and N_2^+ [14–16]. This progress has enabled several further steps in molecular ion quantum control [17–20].

We here extend these techniques by combining buffer gas cooling with QLS and by implementing a state preparation scheme that utilizes both microwave and Raman transitions in the hyperfine structure of the molecular ion. This enables us to perform pure quantum state

* dholzapfel@phys.ethz.ch

† daniel.kienzler@phys.ethz.ch

preparation, coherent control and non-destructive state readout of a single H_2^+ molecule. We demonstrate the capabilities of our platform for precision spectroscopy by performing microwave spectroscopy of a hyperfine transition with a statistical uncertainty of 2 Hz.

The H_2^+ molecule has two identical nuclei which makes it a symmetric, homonuclear molecule. The Pauli principle requires that the molecular wavefunction is antisymmetric under exchange of the two protons. The molecule therefore occurs in two spin isomers: para- H_2^+ with total nuclear spin $I = 0$ and even rotational quantum numbers N , and ortho- H_2^+ with $I = 1$ and odd values of N . We here concentrate on the lowest energy rovibrational state of ortho- H_2^+ with vibrational quantum number $\nu = 0$ and $N = 1$.

We co-trap an H_2^+ ion and a $^9\text{Be}^+$ ion in a linear Paul trap. An ultra-high vacuum chamber with an inner cryogenically cooled chamber houses the trap. For details on the apparatus and experimental techniques see [Methods](#) and Schwegler *et al.* [21]. [Figure 1](#) shows the geometry of the laser beams used to address $^9\text{Be}^+$ and H_2^+ . A beam that is resonant with the D2 transition (wavelength 313 nm) is used for Doppler cooling, state preparation and fluorescence detection of the $^9\text{Be}^+$ ion. A pair of Raman beams (also 313 nm) is used to implement coherent control on the two-level system $|\downarrow\rangle = |F = 2, m_F = 2\rangle$ and $|\uparrow\rangle = |F = 1, m_F = 1\rangle$ in the hyperfine structure of the $^9\text{Be}^+$ electronic ground state. Two infrared laser beams (wavelength 1050 nm) directed at the H_2^+ ion are used to implement stimulated Raman transitions within its hyperfine structure. Both Raman beam pairs can couple the internal degree of freedom of the respective ion to a shared motional mode of the ion pair by driving the corresponding motional sideband. This implements the required operations for motional ground-state cooling and QLS. A microwave antenna located inside the vacuum chamber is used to drive transitions in the hyperfine structure of either ion in a frequency range of 1.2 – 1.4 GHz. Due to the long wavelength of the microwaves and the resulting small Lamb-Dicke parameter no coupling to the ions' motion is possible.

We produce H_2^+ ions using electron-impact ionization of H_2 from the background gas. This results in a wide distribution of vibrational and rotational states [22]. The symmetric, homonuclear nature of H_2^+ causes its rovibrational levels to be extremely long-lived as rovibrational dipole transitions are strongly suppressed [23–25]. While this is a desirable feature for high-precision spectroscopy, it prevents the rotation and vibration from thermalizing on experimental timescales. To solve this issue and prepare our rovibrational target state ($\nu = 0, N = 1$), we utilize helium buffer gas cooling of a single H_2^+ [26, 27]. In our apparatus helium is present in the vacuum chamber at all times and is cooled by collisions with the inner cryogenic chamber. Furthermore, the 313 nm light used for $^9\text{Be}^+$ control dissociates H_2^+ with rates strongly dependent on the vibrational state. Under our experimental conditions, H_2^+ molecules with vibrationally excited

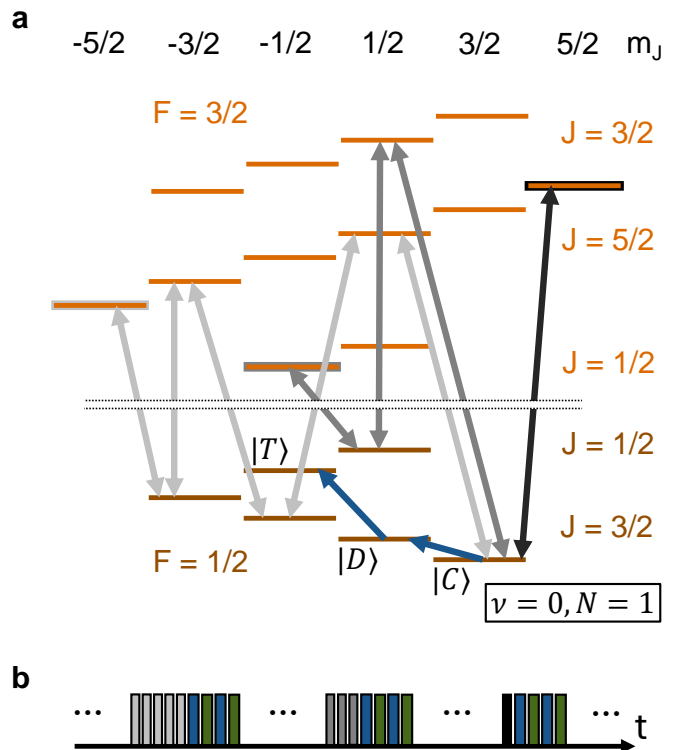


Figure 2. State preparation of ortho- H_2^+ . **a:** Hyperfine and Zeeman structure of ortho- H_2^+ in its vibrational ground state $\nu = 0$ and lowest rotational state $N = 1$. Each of the 18 hyperfine states is labeled with its dominant $|F, J, m_J\rangle$ component. States in the $|F = 1/2\rangle$ manifold are indicated in brown, while orange indicates states in the $|F = 3/2\rangle$ manifold. The energy splittings between the states are not shown to scale. The energy difference between the $F = 1/2$ and $F = 3/2$ manifolds is 1.3 – 1.4 GHz while states within an $|F, J\rangle$ manifold are split by up to 13 MHz at our magnetic bias field of 450 μT . For pure state preparation in the hyperfine manifold, Raman blue sideband transitions (blue arrows) are used to implement irreversible population transfer from $|C\rangle$ via $|D\rangle$ into the target state $|T\rangle$ using QLS operations. Different microwave transition chains connect each state of the hyperfine manifold to the Raman transitions. Three examples of such chains for transferring the population from the states $|3/2, 5/2, -5/2\rangle$ (light gray arrows), $|3/2, 1/2, -1/2\rangle$ (dark gray arrows), and $|3/2, 5/2, 5/2\rangle$ (black arrow) to $|C\rangle$ are shown. **b:** Exemplary state preparation pulse sequences. Each group of pulses pumps the population of one specific state (first $|3/2, 5/2, -5/2\rangle$, second $|3/2, 1/2, -1/2\rangle$, third $|3/2, 5/2, 5/2\rangle$) to the target state $|T\rangle$. Microwaves transfer the population from the starting state to $|C\rangle$. Then, Raman blue sideband transitions on H_2^+ (blue) and pulses for implementing dissipation on $^9\text{Be}^+$ (green) pump the population from $|C\rangle$ via $|D\rangle$ to $|T\rangle$. Relative pulse times are not shown to scale.

states of $\nu \geq 2$ are expected to have a lifetime of less than one second, while $\nu = 1$ and $\nu = 0$ have lifetimes of a few minutes and several days, respectively [28, 29]. Thus, H_2^+ with $\nu \geq 2$ is dissociated before buffer gas cooling has a significant impact [27].

Based on the time it takes to observe the first quantum logic signal of the $\nu = 0, N = 1$ hyperfine structure (see below) after H_2^+ is loaded, we estimate an approximate duration of $\mathcal{O}(10 \text{ min})$ for the rovibrational state to be cooled to the ground state. In some instances we lose H_2^+ within this duration. We attribute this loss to dissociation of the $\nu = 1$ state due to 313 nm laser light before buffer gas cooling to $\nu = 0$ could occur. For approximately half of the H_2^+ molecules loaded, we do not observe a quantum logic signal after ten minutes. This is consistent with our expectation of loading either para- or ortho- H_2^+ at random, because currently only ortho- H_2^+ is controlled by our quantum logic scheme.

After the rovibrational state $\nu = 0, N = 1$ is prepared, its hyperfine structure is in a mixed state. [Figure 2.a](#) shows the 18 hyperfine states. We use the angular momentum coupling scheme

$$\mathbf{F} = \mathbf{S}_e + \mathbf{I} \quad \text{and} \quad \mathbf{J} = \mathbf{L} + \mathbf{F}, \quad (1)$$

where \mathbf{S}_e is the electron spin, \mathbf{I} is the total nuclear spin, and \mathbf{L} is the total orbital angular momentum [30]. Since we work with H_2^+ in its electronic ground state, \mathbf{L} is equal to the rotational angular momentum \mathbf{N} . At a finite magnetic field, neither F nor J are good quantum numbers. However, at our magnetic bias field of 450 μT , each hyperfine state has one strongly dominant $|F, J, m_J\rangle$ component, and we use this component to label the state. The frequency difference between the $F = 1/2$ and $F = 3/2$ manifolds is 1.3 – 1.4 GHz while states within an $|F, J\rangle$ manifold are split by up to 13 MHz.

To prepare H_2^+ in a pure quantum state, we employ a state preparation sequence that uses quantum logic operations and collects the population from all hyperfine states into the target state $|T\rangle = |F = 1/2, J = 1/2, m_J = -1/2\rangle$. For all QLS operations we use the ${}^9\text{Be}^+$ hyperfine states $|\downarrow\rangle$ and $|\uparrow\rangle$ and the ion pair’s axial out-of-phase mode of motion (with Fock states $|n\rangle$). For the QLS readout we choose the H_2^+ transition $|T\rangle \leftrightarrow |D\rangle = |1/2, 3/2, 1/2\rangle$, which can be driven as a stimulated Raman transition by the 1050 nm beams and has a frequency of 20.4 MHz. We read out the $|T\rangle$ state population by first performing ground-state cooling of the out-of-phase mode and state preparation on ${}^9\text{Be}^+$, initializing the ion pair and its motion in $|\Psi, \downarrow, n = 0\rangle$, where $|\Psi\rangle$ is the hyperfine state of H_2^+ . In the case that $|\Psi\rangle = |T\rangle$, a red-sideband π -pulse on the H_2^+ $|T\rangle \leftrightarrow |D\rangle$ transition changes the full system’s state from $|T, \downarrow, 0\rangle$ to $|D, \downarrow, 1\rangle$, exciting the shared motion. For $|\Psi\rangle \neq |T\rangle$ the shared motion is not excited. The motional state can be detected using a subsequent red sideband π -pulse and state-dependent fluorescence detection of ${}^9\text{Be}^+$. We call the resulting measurement probability to find ${}^9\text{Be}^+$ in the $|\uparrow\rangle$ state the ‘QLS signal’. It is proportional to the transition probability of the H_2^+ $|T\rangle \leftrightarrow |D\rangle$ transition and thus the $|T\rangle$ state population before the QLS readout sequence.

Within the two-level subsystem $\{|D\rangle, |T\rangle\}$ of H_2^+ , the state $|T\rangle$ can be prepared with a similar pulse sequence,

replacing the red sideband with a blue sideband on the $|D\rangle \leftrightarrow |T\rangle$ transition and performing a repump operation on ${}^9\text{Be}^+$ instead of the fluorescence detection. This pumps the population from the two-level system $\{|D\rangle, |T\rangle\}$ into $|T\rangle$. Pure quantum state preparation can be achieved by relying exclusively on QLS pumping operations, implementing them on the full hyperfine structure as was demonstrated for CaH^+ [15]. This however is hard to achieve for the H_2^+ molecule as matrix elements for Raman transitions connecting the $F = 1/2$ and $F = 3/2$ hyperfine manifolds are at least one order of magnitude weaker than transitions within the $F = 1/2$ manifold. This is a consequence of the Raman transitions only coupling to the orbital angular momentum, not the spins and the F -mixing being weak at our magnetic field.

We solve this issue by implementing stimulated Raman transitions and their motional sideband operations only on two hyperfine transitions ($|C\rangle = |1/2, 3/2, 3/2\rangle \leftrightarrow |D\rangle$ and $|D\rangle \leftrightarrow |T\rangle$, see [Figure 2.a](#)). This two-link chain collects population from the states $|C\rangle$ and $|D\rangle$ into $|T\rangle$. To extend this to all hyperfine states we use microwaves driving magnetic dipole transitions in the hyperfine structure. With sequences of microwave π -pulses we can efficiently connect all levels, but due to the microwave’s long wavelength and corresponding small Lamb-Dicke parameter, they cannot be used to implement the sideband operations required for quantum logic. We therefore alternate microwave operations transferring population from other levels into state $|C\rangle$ and Raman sideband operations that move the population of levels $|C\rangle$ and $|D\rangle$ into $|T\rangle$. The full state preparation sequence consists of 16 repetitions of the $|C\rangle \rightarrow |D\rangle \rightarrow |T\rangle$ chain, with a unique microwave pulse sequence before each repetition. Each of these 15 unique microwave pulse sequences transfers population from a different state to $|C\rangle$. Three examples for such microwave pulse sequences are shown in different shades of gray in [Figure 2.a](#). An exemplary sequence that combines the microwave pulses with QLS operations is shown in [Figure 2.b](#). We compute the optimal sequence to transfer all states to $|T\rangle$ with a shortest-path algorithm [31]. This takes into account that microwave pulses can only perform reversible operations and thus can only be used in the state preparation to transfer population to previously emptied states.

In principle, only one Raman sideband pumping transition combined with microwave sequences is sufficient for the protocol. We however observe lower state preparation contrast using only one transition. This is expected as the ground-state cooling of the ions’ motion is imperfect, leading to a small leakage from $|T\rangle$ to $|D\rangle$. The issue is amplified by the reversible nature of the microwave operations, spreading the leaked population over the full hyperfine structure. Using a second Raman transition suppresses this effect from a linear dependence on the ground-state cooling infidelity for a single Raman transition to a quadratic dependence for two Raman transitions, ‘shielding’ the population in $|T\rangle$.

To test the preparation of $|T\rangle$ we perform the state

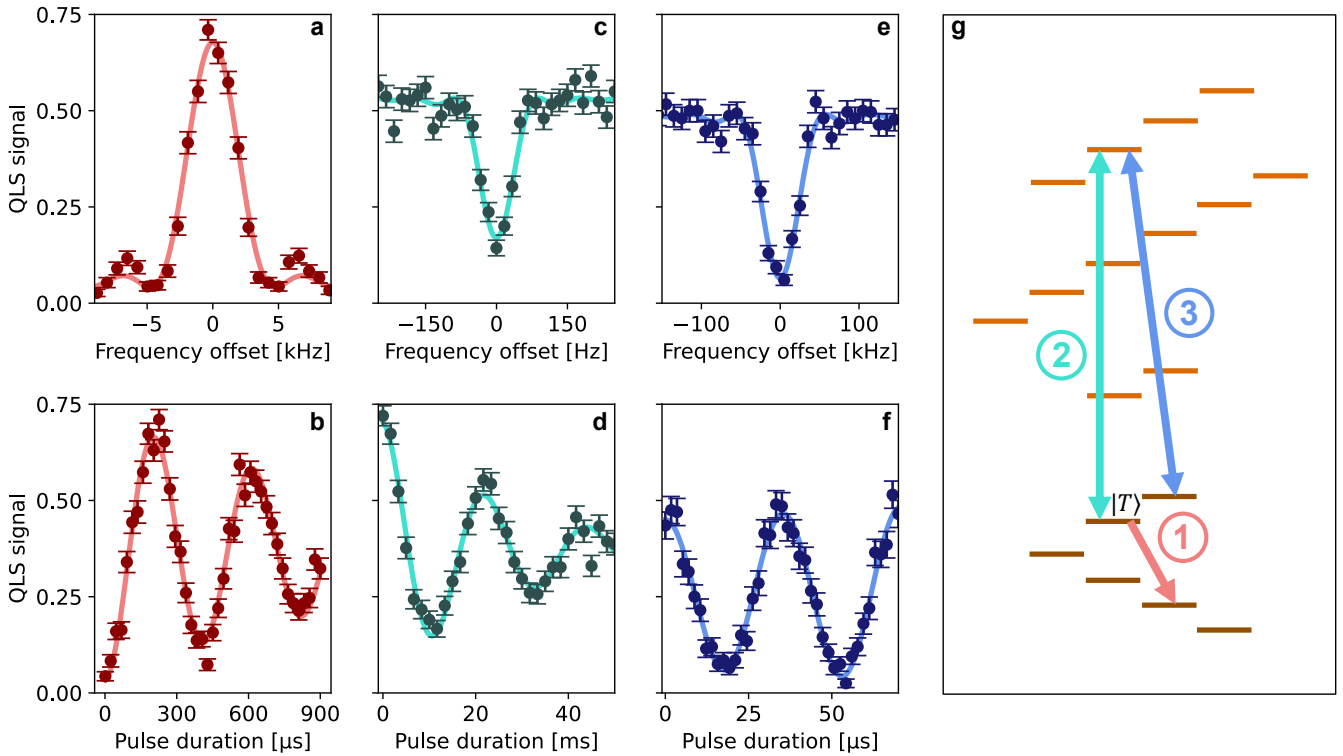


Figure 3. **Coherent manipulation of pure hyperfine states of ortho- H_2^+** . In subfigures a-e, each data point corresponds to 300 repetitions of the respective sequence, and in subfigure f one data point is 200 repetitions. The QLS signal is the probability to find $^9\text{Be}^+$ in the $|T\rangle$ state after the QLS readout and is proportional to the $|T\rangle$ population before QLS readout. Error bars indicate the statistical uncertainty (Standard Error of the Mean, SEM). Solid lines are fits to the data (sinc² function for a,c,e; cosine function with exponential damping for b,d,f). **a, b**: Raman red sideband frequency spectrum (with Raman pulse duration 210 μs) and Rabi oscillations of transition 1. The π -pulse contrast extracted from the fit to the Rabi oscillation data is 0.665(8). **c, d**: Microwave frequency spectrum (microwave pulse duration 11 ms) and Rabi oscillations of the magnetic field insensitive transition 2 using QLS readout on transition 1. **e, f**: Microwave frequency spectrum (microwave pulse duration 17.4 μs) and Rabi oscillations of transition 3 using QLS readout on transition 1 and π -pulses on transition 2 to connect transition 3 to transition 1. The fits result in center frequencies of 20.426 37(5) MHz for transition 1, 1392.081 049(2) MHz for transition 2 and 1391.3083(8) MHz for transition 3. **g**: Schematic of the hyperfine structure of the rovibrational ground state of ortho- H_2^+ indicating transitions 1, 2 and 3.

preparation sequence followed by the quantum logic readout of the $|T\rangle$ state population on the $|T\rangle \leftrightarrow |D\rangle$ transition (transition 1 in Figure 3.g), as described above. We perform a frequency and pulse duration scan of the H_2^+ red sideband operation used in the QLS readout, shown in Figures 3.a and b, demonstrating Rabi oscillations between the levels $|T\rangle$ and $|D\rangle$. From the Rabi oscillation data, we extract a π -pulse contrast of 0.665(8), which corresponds to the combined state-preparation and readout fidelity. Additionally performing a postselection of the data based on a heralding detection, we achieve an improved contrast of 0.74(1) (see Methods for details and postselected data). The decay of the Rabi oscillations is consistent with averages of Debye-Waller couplings to the non-ground state cooled radial modes of motion [13].

To demonstrate the spectroscopy capability of our method, we prepare the state $|T\rangle$ and perform microwave spectroscopy on the $|T\rangle \leftrightarrow |3/2, 3/2, -1/2\rangle$ transition (transition 2 in Figure 3.g). The data is shown in Figure 3.c and d. The readout is again performed with

QLS, probing the population of $|T\rangle$ on transition 1. At our chosen magnetic field, the frequency of transition 2 has only a weak dependence on the magnetic field ($-31 \text{ Hz}/\mu\text{T}$) [30], which allows us to coherently drive the transition with a 11 ms π -pulse, resulting in a Fourier-limited linewidth of 80 Hz. By averaging for half an hour we achieve a statistical uncertainty of 2 Hz which corresponds to a relative uncertainty of 1×10^{-9} . The decay of the Rabi oscillations (Figure 3.d) is consistent with the combined heating of the in-phase axial and radial modes of motion during the microwave probe pulse.

To prepare other hyperfine states and perform spectroscopy of hyperfine transitions which do not include the initial state $|T\rangle$, it is possible to add a sequence of microwave π -pulses after the preparation of $|T\rangle$. We demonstrate this by performing spectroscopy on the $|3/2, 3/2, -1/2\rangle \leftrightarrow |1/2, 1/2, 1/2\rangle$ transition (transition 3 in Figure 3.g). We first prepare $|T\rangle$, followed by a microwave π -pulse on transition 2, transferring the population to $|3/2, 3/2, -1/2\rangle$. We then drive transition 3

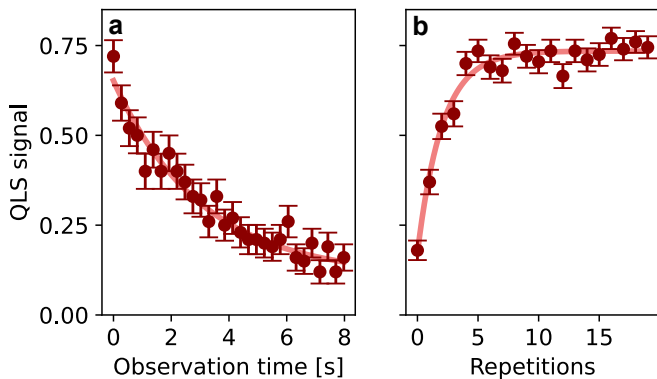


Figure 4. **Ortho- H_2^+ hyperfine state loss and recovery.** The QLS signal is the probability to find $^9\text{Be}^+$ in the $|\uparrow\rangle$ state after the QLS readout and is proportional to the $|T\rangle$ population before QLS readout. **a:** Loss of the $|T\rangle$ state population over time. The H_2^+ ion is initially prepared in the state $|T\rangle$. After this the state is repeatedly probed with QLS readout for up to 8 sec. The full procedure is repeated 100 times and each data point corresponds to the average at a given duration after the state preparation, with error bars indicating the statistical uncertainty (SEM). We extract a $1/e$ lifetime of $3.1(6)$ s from an exponential fit to the data (solid line). **b:** Number of state preparation sequence repetitions required to prepare the H_2^+ molecule in state $|T\rangle$. Initially, a wait time of 10 s allows collisions with background gas to randomize the hyperfine state of the H_2^+ molecule. Subsequently, we apply the state preparation sequence a given number of times and read out the population of $|T\rangle$. Fitting an exponential function (solid line), we find the $1/e$ value to be $2.1(2)$ repetitions. Each data point is the average of 200 repetitions of the sequence, with error bars indicating the statistical uncertainty (SEM).

and return the residual population of $|3/2, 3/2, -1/2\rangle$ to $|T\rangle$ with another transition 2 microwave π -pulse followed by QLS readout of $|T\rangle$. The data is shown as a function of the duration and frequency of the pulse on transition 3 in Figure 3.e and f.

To investigate hyperfine state changes over time we prepare state $|T\rangle$ and repeatedly probe it for a duration of up to 8 s without re-preparation. The results are shown in Figure 4.a. The data follows an exponential decay, and we extract a $1/e$ lifetime of $3.1(6)$ s from the fit. All data presented in this article was taken at a cryostat temperature of 10 K. We have however observed a variation in the $1/e$ lifetime for different cryostat temperatures and different durations after ion loading. This suggests a dependence of the hyperfine state lifetime on the helium pressure. We suspect that cyro-adsorbed helium is released during the electron-impact ionization of

H_2 and then slowly cryogenically pumped without reaching a steady state for several hours. As a complimentary indication of such behaviour we have observed that the rate at which the two ions swap positions along the trap axis decreases with lower cryostat temperatures, which is consistent with a lower pressure. We suspect that the hyperfine state changes are caused either by the collisions directly or by the collisions driving the molecule out of the RF null of the Paul trap and thereby enhancing off-resonantly driven hyperfine transitions by the RF field [32].

Similarly, we can examine the performance of the H_2^+ hyperfine state preparation. For this we wait for a fixed duration of 10 s to ensure a random initial state. Thereafter, we run the state preparation sequence a given number of times and probe the achieved population of the state $|T\rangle$ (see Figure 4.b). The QLS signal increases for increasing numbers of state preparation sequence repetitions and saturates after approximately five repetitions. From an exponential fit, we extract a $1/e$ value of the state recovery of $2.1(2)$ repetitions.

An obvious next step is to perform high-precision hyperfine spectroscopy of the $\nu = 0, N = 1$ state. Beyond this, our work paves the way for a broader range of future high-precision studies of the H_2^+ structure. The state-preparation scheme can be used as a starting point to implement single-ion laser spectroscopy of the H_2^+ rovibrational structure. For selected transitions this is projected to reach a relative uncertainty of $10^{-16} - 10^{-17}$, three to four orders of magnitude beyond the state of the art, which provides the experimental sensitivity to improve the uncertainty of several fundamental constants such as the proton-electron mass ratio significantly [10–12]. The uncertainty for vibrational, rotational, and hyperfine spectroscopy will likely outperform the current uncertainty of the theory. Therefore, theory improvements and spectroscopy schemes that suppress the theoretical uncertainty will be of high importance to harness the potential of this platform [33]. The techniques we have demonstrated in this study are not limited to H_2^+ and can be implemented for other molecular ion species. They can be directly applied to the other homonuclear isotopologues of the hydrogen molecular ion D_2^+ and T_2^+ .

The authors thank J. C. J. Koelemeij and J.-Ph. Karr for helpful discussions and the Segtrap and Penning teams of the ETHZ TIQI group for sharing laser light. This work was supported by Swiss National Science Foundation Grant No. 179909 and 212641, as well as ETH Research Grant No. ETH-52 19-2.

[1] V. I. Korobov, L. Hilico, and J.-P. Karr, Fundamental transitions and ionization energies of the hydrogen molecular ions with few ppt uncertainty, *Phys. Rev. Lett.* **118**,

233001 (2017).

[2] S. Schiller, Precision spectroscopy of molecular hydrogen ions: an introduction, *Contemporary Physics* **63**, 247

- (2022).
- [3] P. O. Schmidt, T. Rosenband, C. Langer, W. M. Itano, J. C. Bergquist, and D. J. Wineland, Spectroscopy using quantum logic, *Science* **309**, 749 (2005).
 - [4] C. Delaunay, J.-P. Karr, T. Kitahara, J. C. J. Koelemeij, Y. Soreq, and J. Zupan, Self-consistent extraction of spectroscopic bounds on light new physics, *Phys. Rev. Lett.* **130**, 121801 (2023).
 - [5] S. Schiller and J.-P. Karr, Prospects for the determination of fundamental constants with beyond-state-of-the-art uncertainty using molecular hydrogen ion spectroscopy, *Phys. Rev. A* **109**, 042825 (2024).
 - [6] I. Doran, N. Hölsch, M. Beyer, and F. Merkt, Zero-quantum-defect method and the fundamental vibrational interval of H_2^+ , *Phys. Rev. Lett.* **132**, 073001 (2024).
 - [7] M. R. Schenkel, S. Alighanbari, and S. Schiller, Laser spectroscopy of a rovibrational transition in the molecular hydrogen ion H_2^+ , *Nature Physics* **20**, 383 (2024).
 - [8] N. Huntemann, C. Sanner, B. Lipphardt, C. Tamm, and E. Peik, Single-ion atomic clock with 3×10^{-18} systematic uncertainty, *Phys. Rev. Lett.* **116**, 063001 (2016).
 - [9] S. M. Brewer, J.-S. Chen, A. M. Hankin, E. R. Clements, C.-W. Chou, D. J. Wineland, D. B. Hume, and D. R. Leibbrandt, $^{27}\text{Al}^+$ quantum-logic clock with a systematic uncertainty below 10^{-18} , *Phys. Rev. Lett.* **123**, 033201 (2019).
 - [10] D. Bakalov and S. Schiller, The electric quadrupole moment of molecular hydrogen ions and their potential for a molecular ion clock, *Applied Physics B* **114**, 213 (2014).
 - [11] S. Schiller, D. Bakalov, and V. I. Korobov, Simplest molecules as candidates for precise optical clocks, *Phys. Rev. Lett.* **113**, 023004 (2014).
 - [12] J.-P. Karr, S. Patra, J. C. J. Koelemeij, J. Heinrich, N. Sillitoe, A. Douillet, and L. Hilico, Hydrogen molecular ions: new schemes for metrology and fundamental physics tests, *Journal of Physics: Conference Series* **723**, 012048 (2016).
 - [13] D. J. Wineland, C. Monroe, W. M. Itano, D. Leibfried, B. E. King, and D. M. Meekhof, Experimental issues in coherent quantum-state manipulation of trapped atomic ions, *J. Res. Natl. Inst. Stand. Technol.* **103**, 259 (1998).
 - [14] F. Wolf, Y. Wan, J. C. Heip, F. Gebert, C. Shi, and P. O. Schmidt, Non-destructive state detection for quantum logic spectroscopy of molecular ions, *Nature* **530**, 457 (2016).
 - [15] C.-W. Chou, C. Kurz, D. B. Hume, P. N. Plessow, D. R. Leibbrandt, and D. Leibfried, Preparation and coherent manipulation of pure quantum states of a single molecular ion, *Nature* **545**, 203 (2017).
 - [16] M. Sinhal, Z. Meir, K. Najafian, G. Hegi, and S. Willitsch, Quantum-nondemolition state detection and spectroscopy of single trapped molecules, *Science* **367**, 1213 (2020).
 - [17] C.-W. Chou, A. L. Collopy, C. Kurz, Y. Lin, M. E. Harding, P. N. Plessow, T. Fortier, S. Diddams, D. Leibfried, and D. R. Leibbrandt, Frequency-comb spectroscopy on pure quantum states of a single molecular ion, *Science* **367**, 1458 (2020).
 - [18] Y. Lin, D. R. Leibbrandt, D. Leibfried, and C.-W. Chou, Quantum entanglement between an atom and a molecule, *Nature* **581**, 273 (2020).
 - [19] A. L. Collopy, J. Schmidt, D. Leibfried, D. R. Leibbrandt, and C.-W. Chou, Effects of an oscillating electric field on and dipole moment measurement of a single molecular ion, *Phys. Rev. Lett.* **130**, 223201 (2023).
 - [20] Y. Liu, J. Schmidt, Z. Liu, D. R. Leibbrandt, D. Leibfried, and C.-W. Chou, Quantum state tracking and control of a single molecular ion in a thermal environment (2023).
 - [21] N. Schwegler, D. Holzapfel, M. Stadler, A. Mitjans, I. Sergachev, J. P. Home, and D. Kienzler, Trapping and ground-state cooling of a single H_2^+ , *Phys. Rev. Lett.* **131**, 133003 (2023).
 - [22] Y. Weijun, R. Alheit, and G. Werth, Vibrational population of H_2^+ after electroionization of thermal H_2 , *Zeitschrift für Physik D Atoms, Molecules and Clusters* **28**, 87 (1993).
 - [23] H. O. Pilón, Quadrupole transitions in the bound rotational-vibrational spectrum of the deuterium molecular ion, *Journal of Physics B: Atomic, Molecular and Optical Physics* **46**, 245101 (2013).
 - [24] D. M. Bishop, S. Shih, C. L. Beckel, F. Wu, and J. M. Peek, Theoretical study of H_2^+ spectroscopic properties. iv. adiabatic effects for the $2p\pi_u$ and $3d\sigma_g$ electronic states, *The Journal of Chemical Physics* **63**, 4836 (1975).
 - [25] V. I. Korobov and D. Bakalov, Forbidden ortho-para electric dipole transitions in the H_2^+ ion, *Phys. Rev. A* **107**, 022812 (2023).
 - [26] A. K. Hansen, O. O. Versolato, L. Klosowski, S. B. Kristensen, A. Gingell, M. Schwarz, A. Windberger, J. Ullrich, J. R. C. López-Urrutia, and M. Drewsen, Efficient rotational cooling of coulomb-crystallized molecular ions by a helium buffer gas, *Nature* **508**, 76 (2014).
 - [27] S. Schiller, I. Kortunov, M. Hernández Vera, F. Gianturco, and H. da Silva, Quantum state preparation of homonuclear molecular ions enabled via a cold buffer gas: An ab initio study for the H_2^+ and the D_2^+ case, *Phys. Rev. A* **95**, 043411 (2017).
 - [28] G. H. Dunn, Photodissociation of H_2^+ and D_2^+ : Theory, *Phys. Rev.* **172**, 1 (1968).
 - [29] J.-P. Karr (2024), private communication.
 - [30] J.-P. Karr, V. I. Korobov, and L. Hilico, Vibrational spectroscopy of H_2^+ : Precise evaluation of the Zeeman effect, *Phys. Rev. A* **77**, 062507 (2008).
 - [31] O. Stadler, State preparation and readout routine for molecular ions, *Master's Thesis, ETH Zürich* (2023).
 - [32] M. Hernández Vera, F. A. Gianturco, R. Wester, H. da Silva, O. Dulieu, and S. Schiller, Rotationally inelastic collisions of H_2^+ ions with He buffer gas: Computing cross sections and rates, *The Journal of Chemical Physics* **146**, 124310 (2017).
 - [33] S. Schiller and J.-P. Karr, Prospects for the determination of fundamental constants with beyond-state-of-the-art uncertainty using molecular hydrogen ion spectroscopy, *Phys. Rev. A* **109**, 042825 (2024).
 - [34] J. B. Wübbena, S. Amairi, O. Mandel, and P. O. Schmidt, Sympathetic cooling of mixed-species two-ion crystals for precision spectroscopy, *Phys. Rev. A* **85**, 043412 (2012).
 - [35] D. J. Gorman, P. Schindler, S. Selvarajan, N. Daniilidis, and H. Häffner, Two-mode coupling in a single-ion oscillator via parametric resonance, *Phys. Rev. A* **89**, 062332 (2014).
 - [36] V. I. Korobov, L. Hilico, and J.-P. Karr, Hyperfine structure in the hydrogen molecular ion, *Phys. Rev. A* **74**, 040502 (2006).
 - [37] J.-P. Karr, F. Bielsa, A. Douillet, J. Pedregosa Gutierrez, V. I. Korobov, and L. Hilico, Vibrational spectroscopy of H_2^+ : Hyperfine structure of two-photon transitions, *Phys.*

- [Rev. A **77**, 063410 \(2008\)](#).
- [38] J.-P. Karr, M. Haidar, L. Hilico, Z.-X. Zhong, and V. I. Korobov, Higher-order corrections to spin-spin scalar interactions in HD^+ and H_2^+ , [Phys. Rev. A **102**, 052827 \(2020\)](#).
- [39] M. Haidar, V. I. Korobov, L. Hilico, and J.-P. Karr, Higher-order corrections to spin-orbit and spin-spin tensor interactions in hydrogen molecular ions: Theory and application to H_2^+ , [Phys. Rev. A **106**, 022816 \(2022\)](#).

METHODS

I. Apparatus and ion control. Our apparatus, ion loading procedure, H_2^+ lifetimes and motional ground-state cooling are described in detail in [21]. Some key features are summarized in the following. Additionally, we will point out significant changes and additions to the apparatus.

The trap is a micro-fabricated monolithic linear Paul trap with an electrode-ion distance of 300 μm . It is operated at a frequency of 78.5 MHz. The motional frequencies of the axial in- and out-of-phase modes of the $\text{H}_2^+ - {}^9\text{Be}^+$ ion crystal are 1.3 MHz and 3.4 MHz, respectively. Due to the high mass ratio of the two ions, their radial motion is only very weakly coupled [34]. We can, therefore, allocate each of the radial motional modes to primarily one of the two ions. The two out-of-phase radial modes where primarily the ${}^9\text{Be}^+$ ion moves have frequencies 1.7 MHz and 1.9 MHz, the modes dominated by H_2^+ are the in-phase modes at 9.6 MHz and 9.8 MHz.

The usual control sequence to prepare both the motional and the internal states of the two ions is: Doppler cooling of ${}^9\text{Be}^+$ and initialization of ion order, optical dipole force gradient (ODF) assisted Doppler cooling (Section II) of the H_2^+ dominated radial motional modes, ground-state cooling of the axial motional modes, ${}^9\text{Be}^+$ state preparation to $|\downarrow\rangle = |F=2, m_F=2\rangle$, H_2^+ hyperfine state preparation (Section III) to $|T\rangle$, QLS detection to optionally herald (Section IV) the preparation of state $|T\rangle$, re-cooling of all motional modes (including Doppler cooling, ODF assisted Doppler cooling and axial ground-state cooling), ${}^9\text{Be}^+$ state preparation, H_2^+ state reset after heralding detection, experiment-specific pulses, QLS detection. Details on each step can be found below or in [21].

The laser beam geometry is shown in Figure 1. The 313 nm beams manipulating ${}^9\text{Be}^+$ are focused to a beam waist radius of $\approx 10 \mu\text{m}$ for the Resonant beam and $\approx 16 \mu\text{m}$ for the two Raman beams BR1 and BR2. The Raman beams are detuned from the D2 transition by 42 GHz. The 1050 nm beams (HR1 and HR2) used for manipulating H_2^+ have a power of $\approx 400 \text{ mW}$ each and are focused to a beam waist radius of $\approx 5 \mu\text{m}$ at the ion's position. HR1 has π polarization while the polarization of HR2 is set approximately half way between π and $(\sigma_+ + \sigma_-)$. Driving the stimulated Raman transitions in the H_2^+ hyperfine structure requires polarization $(\sigma_+ + \sigma_-)$ while the ODF assisted Doppler cooling requires π polarization. The setting used here is a compromise to enable both operations within the same sequence.

II. Optical dipole force gradient assisted Doppler cooling. The two in-phase radial modes of motion only weakly couple to the ${}^9\text{Be}^+$ ion and do not thermalize close to the Doppler limit when Doppler cooling ${}^9\text{Be}^+$. We developed a technique to parametrically couple these modes to a coolable motional mode by means of an ODF that implements a population swapping interaction between the motional modes. The technique

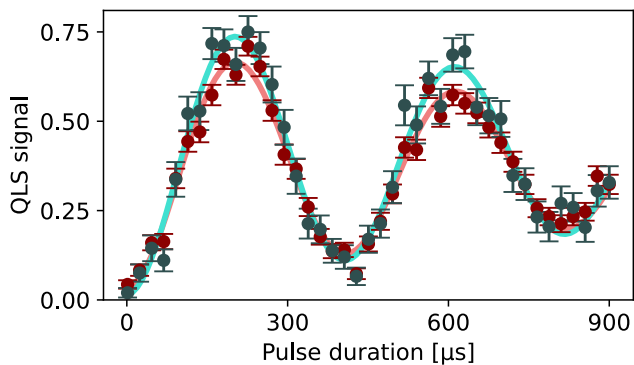
is a modification of the cooling technique demonstrated by Gorman *et al.* [35], replacing the modulation of a trap voltage with a modulated optical potential. For this, we use the HR1 and HR2 laser beams described above. For equal linear polarization of the beams and a relative frequency difference δ , they produce a walking standing wave at the H_2^+ ion's position, resulting in a modulation of the trap potential with frequency δ . For a frequency difference equal to the difference of two motional modes, this implements a parametric coupling between the two modes, causing resonant exchange of their motional excitation. We use this to swap the excitation of the in-phase radial modes with the Doppler cooled axial in-phase mode, thereby cooling the radial modes. This technique and its extension to ground-state cooling will be presented in detail in a future publication.

Since the HR1 and HR2 k -vector difference has a projection onto the radial modes of motion, motional excitation of these spectator modes results in poor contrast of the Raman transitions on H_2^+ due to the Debye-Waller effect [13]. We observe that the ODF assisted Doppler cooling of the H_2^+ radial modes is required to achieve the fidelity of H_2^+ hyperfine state preparation and QLS. This effect could be reduced by adjusting the beam geometry such that the k -vector difference of the Raman beams is parallel to the trap axis.

III. H_2^+ hyperfine state preparation. To prepare the hyperfine state of H_2^+ in a pure quantum state, we combine two QLS pumping steps ($|C\rangle \rightarrow |D\rangle \rightarrow |T\rangle$) with many microwave transitions, to transfer population from the entire hyperfine structure to $|C\rangle$. Frequency values for the microwave pulses in the state preparation are calculated by numerical diagonalization of the combined hyperfine and Zeeman Hamiltonian at our chosen bias magnetic field of 450 μT [30, 36, 37] using the recently improved theoretical hyperfine interaction coefficients [38, 39]. Microwave π -times were measured for three microwave transitions with $\Delta m_J = -1, 0, 1$, respectively, and are calculated for all other transitions by scaling the π -times with the ratios of the calculated transition dipole moments. Frequencies of the Raman motional sideband transitions are calibrated regularly to compensate for drifts of the axial out-of-phase mode frequency and the laser beam intensity causing AC Stark shifts.

To improve the fidelity of the state preparation we repeat pulses involved in QLS in a specific manner. We drive a blue-sideband π -pulse on the $|D\rangle \rightarrow |T\rangle$ transition of H_2^+ , followed by a block of a red-sideband π -pulse and a spin-state repumping sequence on ${}^9\text{Be}^+$ that is repeated twice. This set of pulses is repeated a second time to complete a single QLS pumping step $|D\rangle \rightarrow |T\rangle$. The same sequence is used for $|C\rangle \rightarrow |D\rangle$. To pump the population from any hyperfine state to $|T\rangle$, the sequence is as follows: State-specific sequence of microwave π -pulses to transfer the population to $|C\rangle$, $|C\rangle \rightarrow |D\rangle$, $|D\rangle \rightarrow |T\rangle$, $|C\rangle \rightarrow |D\rangle$, $|D\rangle \rightarrow |T\rangle$.

The required microwave pulse sequences for addressing



Extended Data Figure 1. **Heralded quantum logic spectroscopy signal of ortho- H_2^+** . The QLS signal is the probability to find ${}^9\text{Be}^+$ in the $|\uparrow\rangle$ state after the QLS readout and is proportional to the $|T\rangle$ population before QLS readout. The red data is the full data taking all 300 repetitions into account, as presented in Figure 3.b. The turquoise data is post-selected based on the herald detection. This leads to an average of ≈ 100 repetitions being considered in each data point. Error bars indicate the statistical uncertainty (SEM) for the corresponding repetitions per data point. Solid lines are fits to the data (cosine functions with exponential damping). The contrast is improved from 0.665(8) to 0.74(1) by post selecting the raw data.

the entire hyperfine structure are found using a shortest path algorithm on a directed graph, where the nodes represent populations among the hyperfine states and weighted edges represent possible operations and their duration. The hyperfine states are encoded as binary vectors where a 1(0) indicates non-zero(zero) population present. Microwave π -pulses can swap the population of two states and therefore swap a 0 and a 1. A QLS pumping step can combine two populations into one, combining two 1's into a single 1 and a new 0. Initially, the algorithm assumes population everywhere (all 1's). The algorithm finds the shortest path to the graph node where the target state is the only one populated. More details can be found in [31].

The H_2^+ hyperfine state preparation sequence consists of ≈ 100 pulses on H_2^+ and ≈ 400 pulses on ${}^9\text{Be}^+$, with a total duration of 65 ms. All Doppler cooling, ground state cooling, ${}^9\text{Be}^+$ state preparation and fluorescent readout pulses described above take an additional 85 ms, resulting in a full sequence length of 150 ms.

IV. Heralding and post-selection. In the data presented in the main text, we do not perform any post-selection. We can, however, perform a heralding measurement after the state-preparation, and before the actual measurement, that makes it possible to select only the data points where the H_2^+ ion was in the correct hyperfine state. The unheralded data is shown in Figure 3.b and again in Extended Data Figure 1 in red. The herald flags if the $|T\rangle$ state was successfully prepared in each experimental run. We post-select the data based on ‘positive’ herald detections. This results in a post-selected

state-preparation fidelity. The post-selection increases the contrast from 0.665(8) to 0.74(1). The heralded data is shown in Extended Data Figure 1 in turquoise.

The heralding measurement drives population from $|T\rangle$ to $|D\rangle$. Therefore, we reset the hyperfine state to $|T\rangle$ by performing QLS pumping on $|D\rangle \rightarrow |T\rangle$ after the heralding measurement and before the actual measurement.